OXFORD

Cerebral Cortex, 2024, **34**, bhae416
https://doi.org/10.1093/cercor/bhae416
Original Article

Cortical development in the structural model and free energy minimization

James Wright [1,*], Paul Bourke[2]

[1]Centre for Brain Research and Department of Psychological Medicine, School of Medicine, University of Auckland, 85 Park Road, Grafton, Auckland, New Zealand
[2]Centre for Brain Research, School of Medicine, University of Auckland, 85 Park Road, Grafton, Auckland, New Zealand
*Corresponding author: James Wright, Centre for Brain Research and Department of Psychological Medicine, School of Medicine, University of Auckland, Auckland, New Zealand. Email: jj.w@xtra.co.nz

A model of neocortical development invoking Friston's Free Energy Principle is applied within the Structural Model of Barbas et al. and the associated functional interpretation advanced by Tucker and Luu. Evolution of a neural field with Hebbian and anti-Hebbian plasticity, maximizing synchrony and minimizing axonal length by apoptotic selection, leads to paired connection systems with mirror symmetry, interacting via Markov blankets along their line of reflection. Applied to development along the radial lines of development in the Structural Model, a primary Markov blanket emerges between the centrifugal synaptic flux in layers 2,3 and 5,6, versus the centripetal flow in layer 4, and axonal orientations in layer 4 give rise to the differing shape and movement sensitivities characteristic of neurons of dorsal and ventral neocortex. Prediction error minimization along the primary blanket integrates limbic and subcortical networks with the neocortex. Synaptic flux bypassing the blanket triggers the arousal response to surprising stimuli, enabling subsequent adaptation. As development progresses ubiquitous mirror systems separated by Markov blankets and enclosed blankets-within-blankets arise throughout neocortex, creating the typical order and response characteristics of columnar and noncolumnar cortex.

Key words: free energy principle; predictive coding; Markov blankets; cortical development; structural model.

Introduction

In this paper, we try to provide a principled account of the symmetries in functional brain architectures that emerge in neurodevelopment, utilizing simple neuroplasticity rules and applying the free energy principle to self-organization of synaptic flux exchanges.

Analysis of the functional organization of limbic and neocortex has been undertaken by Tucker and Luu (Tucker and Luu 2021; Luu and Tucker 2023; Tucker and Luu 2023), working within the Structural Model of Barbas (1986 and subsequent). This work has been extended in collaboration with Friston (Luu et al. 2024) to incorporate a model of predictive error minimization within each cortical column (Bastos et al. 2012, 2020). The present paper expands these concepts by introducing an explanation of cortical development at the millimetric scale (mesoscale) to account for the structure/function relationships in more general and modular cellular terms.

The structural model and related function

Structure

We will loosely refer to the Structural Model as a theory of cortical embryogenesis and structural differentiation that is a compound of the Structural Model proper, the Dual Origin Theory of cortical embryogenesis, and the recognition of cortical organization in target-like rings.

The Structural Model proper (Barbas 1986; Barbas and Rempel-Clower 1997; Barbas 2015; Garcia-Cabezas et al. 2019, 2020; Sancha-Velasco et al. 2023; Ruiz-Cabrera et al. 2023) describes the relation between the laminar complexity of the cerebral cortex and the laminar pattern of cortico-cortical connections. Synaptic projections from areas of simple laminar architecture to areas of more complex laminar architecture originate from neurons in infragranular 5,6 layers and terminate in supragranular 1/3 layers. Projections from areas of complex laminar architecture projecting to areas of simpler laminar architecture originate in supragranular layers 2,3 and terminate in layers 4,6. Projections connecting areas of comparable laminar complexity originate in both infra- and supragranular layers and terminate across all layers. Cellular and molecular features vary systematically along the cortical gradient of laminar complexity—factors that favor synaptic plasticity including histone-modifying enzymes decrease along the complexity gradient (Sancha-Velasco et al. 2023) while molecular markers that favor neuron stability increase (Garcia-Cabezas et al. 2017).

On phylogenetic grounds, Sanides proposed a Dual Origin of the neocortex (Sanides 1962, 1964, 1970) from two anlagen adjacent to the hippocampal and olfactory allocortices, giving rise to growth expansions in concentric rings of increasing laminar complexity. As cortex is traced radially, the simpler layers give way to neocortex organized in depth as a six-layered structure of mixed excitatory and inhibitory cells, afferent and efferent to subcortical and other cortical areas. Morphogenetic gene expression (Puelles et al. 2019, 2024) follows the radial pattern, and cortical embryogenesis begins later and continues longer in the outer rings of development (Rakic 2002; Barbas and García-Cabezas 2016;

Received: August 26, 2024. **Revised:** September 19, 2024. **Accepted:** October 10, 2024

Garcia-Cabezas et al. 2019). As radial cellular differentiations proceed, cell connectivity also undergoes modification under the distance rule (Markov et al. 2011; Vezoli et al. 2021), favoring cross-connections by shortest and most locally dense pathways—an arrangement facilitating metabolic efficiency and rapid interactions in a "small world." Actual anatomy is a compromise between the radial versus small world arrangements (Aparicio-Rodriguez and Garcia-Cabezas 2023) created as cortico-cortical connections also extend in a circumferential manner along the radial lines. The upshot is that along the radial lines of development, centrifugal signals from the limbic system interact with centripetal signals from special sensory and motor cortex, to some extent bypassing each other in a counterflow between a hub-like center versus primary cortical areas that establish direct sensory and motor interactions with the environment (Adams et al. 2013).

Further order emerges at the millimetric scale. Cells in layers 2,3 and 5,6 also send intracortical excitatory connections laterally over short distances (Levitt et al. 2002). Layer 4 receives ascending cortical inputs including those from the special senses and—crucially for our following arguments—relays these signals preferentially toward the upper layers by superficially directed axons (Shipp 2007; Shipp and Friston 2022). In the upper layers, the superficial patch system (Muir et al. 2011; Muir and Douglas 2011; Martin and Roth 2014) is made up of patches of cells that make lateral connections, skipping from patch to neighboring patches in several steps, and thus forming gridworks apparently organized to distribute information between intracortical locales. Organization is highly variable at mesoscale, and much effort has been made to systematize the appearances (Horton and Adams 2005; Molnar 2020). Some parts of the cortex—notably the primary visual cortex of large animals—are organized in a columnar fashion in which zones of short-axon neurons are surrounded by groups of superficial patch cells, creating macrocolumns, but elsewhere this organization is minimal to apparently absent. Within macrocolumns, individual cells exhibit organization according to the stimulus preferences of cells (e.g. Obermayer and Blasdel 1993). Columnar orderliness or absence depends on species brain size among other factors (Kaschube et al. 2010), but similar neuron response preferences can be detected whether or not columns are present (Meng et al. 2012).

Function

The dual origins from hippocampal and olfactory origins lead to separation of the cortex into dorsal and ventral divisions. Tucker and Luu (2023) argue that these divisions served elementary "go" versus "stop" roles at the most primitive stage of encephalization, and that this functional distinction still underlies the dorsal division's initiation of actions and control of internally directed attention and implicit memory, versus the ventral division's association with alerting responses to novel sensory material and recall of explicit memories. The divisions are also separate in their relations to the dorsal thalamus (Butler 2008; Cisek 2022), the dorsal division receiving lemnothalamic inputs from spinal lemniscal sources, and the ventral division receiving collothalamic inputs from the midbrain roof. Consequently, cortical activation of the divisions is also separated—the lemnothalamic activation system serving the dorsal division and the collothalamic system the ventral division (Butler 2008; Loonen and Ivanova 2016). The two activation systems differ in predominance of modulating neurotransmitters (Hansen et al. 2022, Froudist-Walsh et al. 2023)—the dorsal system depending on noradrenaline, serotonin, and acetylcholine; the ventral on dopamine—and appear to differentially mediate rapid eye movement (REM) sleep and slow-wave sleep (SWS), respectively (reviewed in Tucker et al. 2022). The lemnothalamic inputs drive cortical desynchronization and release capacity for impulsion of overt behavior, and the collothalamic activates the ventral division's response to novelty (Stenberg 2007).

In functional anatomy, neurons in the dorsal and ventral streams differ in their sensitivity to stimulus shape and movement—those of the dorsal system being relatively insensitive to shape and sensitive to movement, and those of the ventral system vice versa (Trevarthan 1968; Ungerleider and Mishkin 1982; Goodale and Milner 1992; Sheth and Young 2016; Yang et al. 2022)—so they are suited to the organization of widespread and coordinated actions, versus recognition of specific objects. Matching this variation, there is evidence that the receptive field size of pyramidal neurons in layers 2,3 decreases along the laminar complexity gradient (Garcia-Cabezas et al. 2018). Notably, the two divisions differ in the thickness of cortical layer 4—the layer receiving special sensory afferents and relaying these toward the cortical surface (Garcia-Carbezas and Barbas 2014; Barbas and Garcia-Carbezas 2015).

We hope to explain the means by which the centrifugal and centripetal flows of information lead to the integration of subcortical and cortical information processing, including the emergence of different neuron preferences for shape and movement in the two divisions. We will relate these to the divisions' reactions to surprise and co-ordination of subsequent responses and go on to show how the same self-organization principles—consequences of the free energy principle and predictive error minimization—account for emergence of the mesoscopic order throughout neocortex. We draw upon our earlier work on the embryogenesis of the cortex at mesoscale (Wright and Bourke 2013, 2016, 2022, 2023, 2024; Wright et al. 2014) initially motivated by an emphasis on neural field dynamics (e.g. Wright and Liley 1996). We argued that apoptotic selection of neurons maximizing synchronous oscillation explains columnar and noncolumnar structure and neuron stimulus response preferences—an argument that implicitly depended on the free energy principle.

The free energy principle

The free energy principle and the concept of prediction error minimization, as advanced by Friston and colleagues (Friston 2002, 2005; Friston 2010a, 2010b, 2022; Friston et al. 2012a, 2012b, 2015, 2020, 2021; Friston and Ao 2012; Buckley et al. 2017; Constant 2021; Palacios et al. 2020; Parr et al. 2022) offers a general framework for self-organizing systems, including brain function as a specific instance. The principle depends upon formal parallels (duals) between laws of nature from the principle of least action to the organization of all inferential systems. Jaynes' maximum entropy principle of optimum statistical information is dual to the laws of thermodynamics, and Bayesian inference (Friston 2010a, 2010b; Ramstead et al. 2022) is dual to both. This implies that a correct explanation of neuronal growth and dynamics is de facto an explanation of information processing. The Bayesian inference (i.e. predictive coding) interpretation afforded by the free energy principle means that the structure, plasticity, and dynamics of the brain can all be explained by minimizing variational free energy or, equivalently, maximizing model evidence—a principle neatly summarized as self-evidencing (Hohwy 2016); namely, gathering and assimilating evidence for a generative model of the sensed world.

Essentially, the principle states that systems evolve until they reach a stable state with minimum residual activity (free energy) not accounted for by interaction with their surrounding

environment. Within any system with a boundary via which it must interact with a surrounding environment, an open steady state must be reached in which equal and opposite signals are continuously exchanged via the boundary so as to maintain a synchronous equilibrium of exchange. This boundary is termed by Friston a Markov blanket (Kirchhoff et al. 2018). For example, our sensory epithelia could be regarded as a Markov blanket for the central nervous system, in which case the brain creates a generative model of the sensed world, thereby mirroring the world's causal architecture (e.g. Friston and Buzsaki 2016).

A Markov blanket is the means by which prediction errors are minimized. Applied to learning and the brain, this means that neuronal and synaptic growth must tend inevitably toward a stable state in which perturbations created by inputs are predicted by the consequences of earlier learning, so that signals generated internally minimize the impact of uninformative current inputs on ongoing activity. At an asymptotic limit (although never reached in life), prediction of new incoming sensory stimuli is exact, subject only to certain formal logical limits (Fields et al. 2024) and variational free energy of critical variables approaches zero. The necessary existence of Markov blankets applies also between brain subsystems, each of which evolves toward prediction of mutual interactions, so an embedding of blankets-within-blankets-within-blankets is to be expected, minimizing prediction errors in multiway interactions. The free energy principle suggests that any neuronal system or subsystem can be described as a model or mirror of other subsystems with which it communicates via a shared Markov blanket, around which we would expect to see a mirror symmetry of some sort in the structure of the coupled subsystems.

A prediction error is a free energy gradient (Friston et al. 2017; Tschacher and Haken 2007). When variational free energy is minimized, these gradients are destroyed and prediction errors are resolved. Generated predictions mirror external perturbations to explain away prediction errors (Fields and Levin 2019; Kiebel and Friston 2011; Levin 2019). This kind of mirroring does not necessarily imply exact physical reflection. There may be a difference in the degrees of freedom across a Markov blanket (Hohwy 2016) and mirroring can transcend scales. We will show that patterns of synaptic flux exchanges in the brain can give rise to patterns of synaptic connectivity that form mirror reflections in a topological sense and act to maximize zero-lag synchrony across their line of mirror reflection. Our arguments will be cast in terms of auto- and cross-correlations of synaptic flux, rather than formal Bayesian terms.

Active inference and affordance: surprise and the breakdown of Markov blankets

Friston introduces two supplementary concepts—namely: Active Inference, as an application of the free energy principle to agents, and refers to processes within the brain that create options for future behavior, higher cognitive processes, and the control of attention and action; and Active Affordance, concerned with the selective amplification of perceptual components most relevant to current intention and motivation. These extensions of self-evidencing go into the realm of anticipation, requiring solution of multiple, sometimes contradictory demands, and imply the necessary breaking and restructure of Markov blankets with associated perturbations of variational free energy.

Friston joins Tucker and Luu in locating the operations of inference and affordance within the structural model (Luu and Tucker 2023), utilizing the canonical model of predictive coding advanced by Bastos et al. (2012, 2020). These models are supplemented by the more general solution here proposed, which offers an explanation of the information flow geometry throughout cortex, in lateral organization as well as cortical depth.

A minimum free energy organizational unit

We begin by describing a hypothetical unit that will emerge as zero variational free energy is approached in a realistic neurodynamic field. The description is summarized from Wright and Bourke (2024), and further mathematical background is given in the Appendix. We will show that this schema plays out repeatedly in different forms throughout development.

Basic assumptions

Cells and presynaptic flux

Features of the structural model essential to the following arguments are shown in Fig. 1. We assume that development in radial layers is determined by autonomous unfolding of the genetic program, with other selective factors, to be discussed, subsequently operating.

Neurons operate close to metabolic limits imposed by their large surface area/volume ratio and high demands for ion pumping (Vergara et al. 2019). Cortical synapses are few compared to the number of contacts made between axons and dendrites, so neurons form a sparse one-to-many network, with weak connectivity per synapse (Perin et al. 2011; Song et al. 2005), and low degree of separation. Closely situated neurons form densely interwoven and interpenetrating networks.

We will focus on minimization of free energy with presynaptic flux as the variable of interest. The n unidirectional flows of presynaptic flux in the developing network can be represented as the n elements of a square matrix, $\Phi(t)$ with elements φ_{ij}, that each represent the presynaptic flux received at the $i-\mathbf{th}$ neuron from the $j-\mathbf{th}$ neuron

$$\Phi(t) = GQ(t) \tag{1}$$

where $G(t)$ is a square matrix operator of presynaptic gains and axo-dendritic conduction times, transforming $Q(t)$, a vector of action potential pulse rates of all neurons. Additive dendritic summation of presynaptic pulses and conversion to action potentials according to a sigmoid relation are assumed, but their details are not critical to our following arguments.

Our aim is to describe the geometrical forms toward which $\Phi(t)$ and $G(t)$ converge during development.

Hebbian plasticity

We assume Hebbian gains follow the unification of fast and slow synaptic learning rules proposed by Izhikevich and Desai (2003) combining short-term plasticity and short-term depression, with the slower and more permanent Bienenstock–Cooper–Monro (BCM) rule, including slow "floating hook" negative feedback. Peak synaptic flux delivered along all pathways of flow is given by

$$\varphi_{ij}\left(t + \tfrac{|i-j|}{v}\right) = \varepsilon_{ij} g_{ij} \rho_{ij} Q_j(t) \tag{2}$$

Q_j is the pulse rate of the $j-\mathbf{th}$ neuron, v is the speed of signal spread, and $\frac{|i-j|}{v}$ is the delay from pulse generation to arrival of peak pulse density at pre-synapses on the $i-\mathbf{th}$ neuron, averaged over all routes, polysynaptic or monosynaptic. Synaptic gains are separated into three timescales, so that $\varepsilon_{ij}, g_{ij}, \rho_{ij}$ are the transient synaptic efficacy, the slow dynamic synaptic gain, and

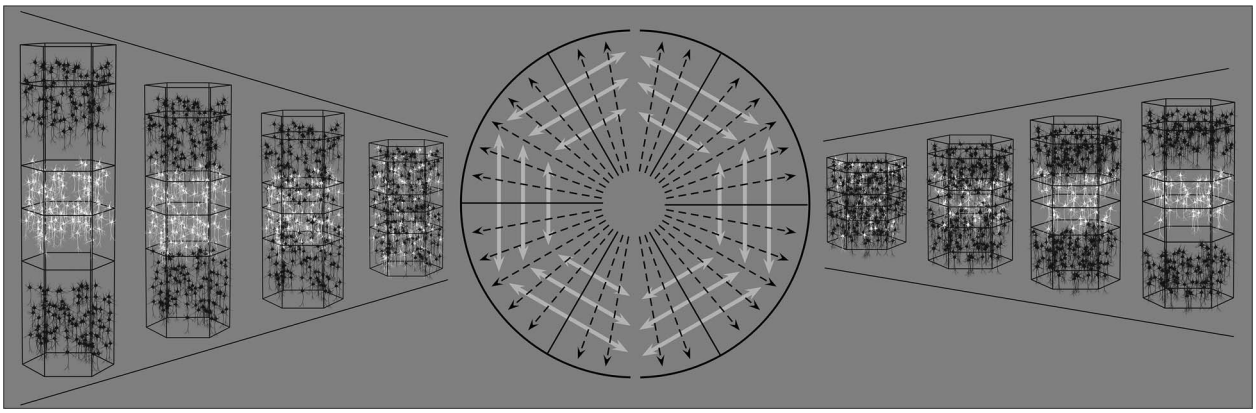

Fig. 1. Essential features of the structural model. With distance from the limbic system, cortical neurons become clustered into more distinct strata in layers 2 and 3, and 5 and 6 (black cells), separated by layer 4 (white cells). Left from center: radial development of cortical layers in the ventral division. Right from center: radial development of cortical layers in the dorsal division. Note greater differentiation of layer 4 in the ventral division. Center: radial development (dashed arrows) progresses from limbic origins to special cortical sensory/motor areas, with lateral intracortical and cortico-cortical connections (gray arrows) also adding circumferential connectivity.

the structural synapse gains along the polysynaptic pathways, respectively—competitive on all three timescales. Synaptic efficacy must lead slower synaptic development, rising with presynaptic flux pulse rate until reaching a transient limit of substrate exhaustion. Slow and structural synapse consolidation become time averages of efficacy.

The functional forms for free energy minimizing processes are usually expressed in terms of gradient flows on variational free energy per se; however, equation (2) emerges under predictive coding or hierarchical Bayesian filtering formulations of self-evidencing when distinguishing between the optimization of precision or synaptic gain and the learning of synaptic connections between predictions and prediction error units (e.g. Bogacz 2017; Friston 2008).

Anti-Hebbian plasticity

Homeostatic mechanisms keep the firing rates of cortical neurons and the balance of excitatory and inhibitory synaptic impulses within stable limits. Anti-Hebbian synaptic plasticity, not yet fully understood, acts to normalize excitatory and inhibitory synaptic gains, while leaving the relative strengths of Hebbian influences unchanged (Keck et al. 2017).

Maximization of synchrony

Developing neurons are selected to maximize zero-lag synchrony and concurrently minimize total axonal length into an ultra-small world configuration. Synchronous firing appears early in neuronal development along with the development of small world connectivity (Downes et al. 2012; Markov et al. 2011; Vergara et al. 2019; Bassett and Bullmore 2006). Concurrent apoptosis (Hollville et al. 2019) favors cells that are firing with zero-lag synchrony (Heck et al. 2008; Sang et al. 2021) apparently because synchrony favors high metabolic turnover and resistance to cell suicide (Vergara et al. 2019).

Development under constraints

Recurrent features of the geometry of presynaptic flux will emerge as features of cortical anatomy. Hebbian plasticity with competition will favor development of monosynaptic connections along preferred pathways. Emergent fields of synchronous firing constitute the spatial eigenmodes of $\Phi(t)$, with remaining connections mediating interactions among the spatial eigenmodes. Convergence to this condition can be explained under the free energy principle, as follows.

Minimization of free energy

As growth proceeds, cell numbers increase as does total presynaptic flux. Hebbian learning forces a fall in the variational free energy of presynaptic flux, F.

$$F = A - C \to 0 \tag{3}$$

Here, A is total presynaptic flux autocorrelation and C is total presynaptic flux cross-correlation (see Appendix). This equation can be also read as *Accuracy* minus *Complexity*, measuring the emergence of structured connectivity.

At the limit at which $F = 0$, it follows that in the exchange of synaptic fluxes φ_{ij} and φ_{ji}, over all synaptic routes between cells at any positions i and j, at all times t and time-lags τ, the sum of their autocorrelations is equal to the sum of their cross-correlations—i.e.:

$$\varphi_{ij}(t)\varphi_{ij}(t-\tau) + \varphi_{ji}(t)\varphi_{ji}(t-\tau) = \varphi_{ij}(t)\varphi_{ji}(t-\tau) + \varphi_{ji}(t)\varphi_{ij}(t-\tau) \tag{4}$$

At this limit, all synaptic fluxes represent the spatial and temporal associations in the network's inputs, and their probability distributions satisfy Bayes theorem—which is what is meant by *self-evidencing*. Steady-state equilibrium requires that energy be equipartitioned—for all i, j, t, τ, $\varphi_{ij}(t) = \varphi_{ij}(t-\tau) = \varphi_{ji}(t) = \varphi_{ji}(t-\tau)$.

Maximization of synchronous oscillation

Selection of neurons that engage in zero-lag synchronous oscillation requires emergence of bidirectional symmetry of exchanged excitation between cells. This results when pairs of excitatory cells, or pairs of inhibitory cells, exchange equal and opposite flux at zero lag ($\tau = 0$), and when pairs of cells, one inhibitory and the other excitatory, fire in antiphase at lag $\tau = \frac{|i-j|}{v}$, i.e. half the period of synchronous oscillation (Chapman et al. 2002; Wright et al. 2000). Thus, zero-lag synchrony is a steady state with energy equipartition and zero variational free energy. Fields of synchrony form the spatial eigenmodes of the network, and coupled interactions of the spatial eigenmodes are described

by asymmetric exchanges of flux that are also solutions of equation (4).

Minimization of prediction error—minimization of perturbation and mirror synchronous fields

Approach to steady state requires minimization of perturbation, but since the system is under continuing input, then where $\Delta\Phi^{+}$ is a vector sum representing flux induced by the externally imposed signals, there must arise an oppositely directed vector sum $\Delta\Phi^{-}$, the compensating synaptic flux required to maximize stability; in effect the neural network predicting and neutralizing its inputs with minimal error, so

$$\Delta\Phi^{+}(t) - \Delta\Phi^{-}(t) \rightarrow 0 \tag{5}$$

That is, the free energy gradients vanish as the free energy is minimized.

Representation of externally imposed and generally time-varying and asymmetrical inputs requires spatial eigenmodes that are coupled by asymmetric and time-varying flux exchanges. Consequently, consistency with relation (5) requires that spatial eigenmodes must develop in paired systems with mirror reversal, each with time-varying flux exchanges between eigenmodes oppositely directed to those in the mirror partner. This concurs with early formulations of self-organization, such as the law of requisite variety; i.e. a system or regulator must have as many internal degrees of freedom as the number of controllable degrees of freedom in its environment. The law of requisite variety can also be viewed in light of the good regulator theorem (Conant and Ashby 1970); namely, every good regulator must be a good model of the system that is being controlled. Thus, each of the paired mirrors is a good regulator of the other.

Excitatory/inhibitory balance—maintenance of a steady state

Steady state requires maintenance of average excitation at a steady level and balances excitatory versus inhibitory flux. That is:

$$\sum \Phi_{e} \rightarrow \sum \varphi_{i} \rightarrow \text{constancy} \tag{6}$$

where $\sum \varphi_{e}$ is the total excitatory presynaptic flux and $\sum \varphi_{i}$ is the total inhibitory presynaptic flux. This stabilization is provided by anti-Hebbian plasticity.

Paired mirror systems must be able to maintain overall excitatory/inhibitory balance, and this can be provided by the collision of traveling waves at the line of interaction of the mirror pair. Since this wave collision permits interaction only of waves orthogonal to the line of wave intersection, overall balance requires multiway interaction of multiple mirror-pair representations.

Mirror-symmetric fields and Markov blankets

Figure 2 left illustrates a system composed of a pair of mirror-symmetric coupled spatial eigenmodes, each of the pair generating oppositely directed, colliding, traveling waves. The diagram shows the topology of the connections and flux exchanges—not a specific topography. The mirror-twin eigenmode systems might be separated by some distance, or their cell soma positions might be interdigitated. At the dashed line, traveling waves can collide.

Interactions at the blanket

Figure 2 right shows how the synchronous fields can interact in the dual system. Paired mirror systems can interact at the line of collision whether cross-connected by excitatory linkages or by inhibitory linkages, and maintenance of balance could take place by either mechanism or their dynamic combination. The asymmetric forms of coupling are those needed to mediate coupling of spatial eigenmodes within each of the dual systems, and also represent episodes of asymmetric exchanges induced by transient perturbation. By shift between the symmetrical excitation, and the symmetrical inhibitory forms of coupling, the dual system can achieve joint excitatory/inhibitory balance. Striking this balance can be mediated in part by the negative feedback "floating hook" property of the BCM learning rule, but the slower mechanisms of anti-Hebbian plasticity are essential to sustain the adjustment.

As junctional exchange manages excitatory/inhibitory balance, prediction error minimization proceeds within each of the mirror duals, and free energy approaches zero. The signals arriving at the junction progressively maximize their mutual information. The mirror-like junction is therefore a Markov blanket, defined by the properties that prediction errors are continuously minimized in the face of recurrent patterns of external input, and although signals are exchanged bidirectionally across the line of mirror reflection, zero-lag synchrony is maintained at the interface. However, never before encountered external perturbations will always cause temporary disruption of the blanket and the passage of a wave of excitation, or of inhibition, across the line of mirror reflection. Thus, the making and breaking of blankets is a part of ongoing function.

The properties of a Markov blanket ascribed here are consistent with earlier theoretical formulations and observations. The dynamics of a Markov blanket can always be expressed in terms of a synchronization manifold (Friston 2019) on which the dynamics of both sides of the blanket evince a generalized synchrony reflecting the mutual predictability and minimization of prediction errors at the Markov blanket. Even when the activity on each side of the blanket is chaotic, when matched to identity on each side, they will be synchronous at zero-lag; very much like that seen empirically (Gollo et al. 2014).

A discussion of the relationship between this explanation of the operation of prediction error minimization versus the canonical model of Bastos et al. (2012, 2020) is deferred to the Conclusion.

Multiway interactions across blankets and redundant representation

Multiway interaction of multiple paired representations, extending some distance across the cortical system, must follow the free energy principle toward maximum joint stability, bringing information in inputs that have differed across the cortex into joint maximization of their mutual information. By further extending to the entire extent of the cortex, prediction errors between brain and environment are minimized.

The generation of multiple mirror systems depends upon redundant storage capacity of cortical synapses. It is shown in the Appendix that as learning develops, the amount of information, including the internal interactions that comprise active inference and active affordance, can become very large, but early in development only simple dual synaptic systems could exist. The largest and simplest scale on which such self-organization could emerge is along the lines of radial development of the neocortex. Multiple mirror-pair subsystems might then develop at diminishing scale. The next section considers how this might take place.

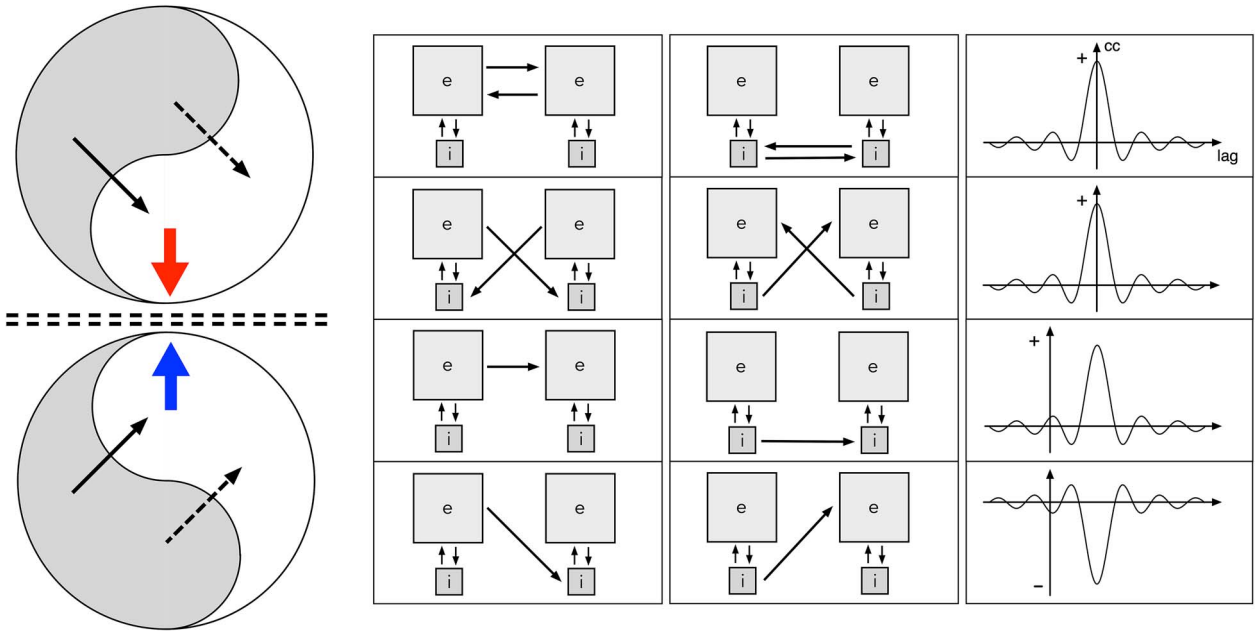

Fig. 2. Left: the topology of neural field interactions meeting requirements for minimization of free energy, minimization of prediction errors, and maintenance of excitatory/inhibitory balance. Within each of a pair of mirror-symmetric systems, spatial eigenmodes (represented arbitrarily as yin-yang figures) interact via excitatory and inhibitory cross-couplings (solid and dashed black lines) generating oppositely directed traveling waves (colored arrows), which collide at the double dashed line of symmetry. Right: exchanges between spatial eigenmodes across the line of wave collision. The gray squares marked **e** and **i** represent clusters of excitatory and inhibitory neurons whose interaction generates fields of synchronous oscillation (spatial eigenmodes). Synapses cross-link to either the excitatory cells, or the inhibitory cells in the neighboring assembly, in one of eight possible symmetrical, or asymmetrical, exchanges. In the left column, these exchanges take place at longer ranges, via efferent excitatory cells. In the middle column, additional exchanges also made possible at short ranges via efferent inhibitory cells are shown. Approximate cross-correlation plots for excitatory cells in each of the paired eigenmodes are shown on the right. These apply to exchanges by excitatory or by inhibitory cross-links, so zero-lag synchrony across the line of wave collision is maintained by all symmetric exchanges and lag synchrony by asymmetric exchanges.

The extension of self-organization within the hierarchical order of the structural model

Counterflows in the radially developing neocortex

Figure 3 shows a series of cortical columns, or domains of cortex with a particular laminar complexity, like those in Fig. 1, indicating the signal flows from higher to lower in the hierarchy along the lines of radial development. Counterflows of synaptic flux develop, limbic flows centrifugally and special neocortical areas centripetally, with the inputs to layer 4 from the special senses imposing a division of flows from the limbic centers. This counterflow constitutes an initial and large-scale instance of roughly mirror-symmetric flows, with preferential direction of flow in layer 4 toward the superficial layers created by that layer's superficially directed axons bringing the counterflows into interaction across a Markov blanket (double dashed line, Fig. 3)—a blanket bringing information of limbic and special sensory origins to self-evidencing exchanges.

Shape and movement sensitivities in developing neurons

The counterflows differ in the dorsal and ventral divisions because of the differing thickness of layer 4 in the ventral division with associated layer 4 deep-to-superficial directed neurons (Shipp 2007). Maximization of synchrony and apoptotic selection of neuron response preferences will differ in the two divisions as a consequence, with subsequent differences in organization of information flows. Where there is a strong deep-to-superficial direction of axons and synaptic flux, competitive processes will favor the emergence of connections in the depth axis, and restrict the development of lateral connections in layers 2,3. This is consistent with the apparent restriction of receptive fields of neurons high in the gradient hierarchy (Garcia-Cabezas et al. 2018). Conversely, with restriction of layer 4 neurons, competition will favor emergence of lateral connectivity to a greater degree and open the cells to a spatially more extensive range of afference.

The Appendix gives a mathematical account of the above consequences for neuron response properties. The neurons with longer lateral spread are less sensitive to detailed spatial structure in their afferent signals and more sensitive to differences of conduction delays from their laterally distributed sources. They are therefore little sensitive to stimulus shapes, but more sensitive to stimulus movements. For the opposite reasons, neurons with less lateral spread of their axons must be more sensitive to differences in shape and less sensitive to movement.

These differences can account not only for the different sensory preferences of the dorsal and ventral divisions, but when the efferent properties of the cells are considered, they are suited to initiate widespread but more precisely timed inputs to other neurons on the one hand versus more spatially restricted and coincident inputs on the other. This explanation of distinction in dorsal versus ventral neuron preferences has consequences for ongoing self-organization as will be discussed later. However, it is not contended that this developmental reason is the sole factor operating. Other reasons for the distinction have been advanced—e.g. Sheth and Young (2016). Such explanations need not be in contradiction, but may be synergic with a primary means of selection.

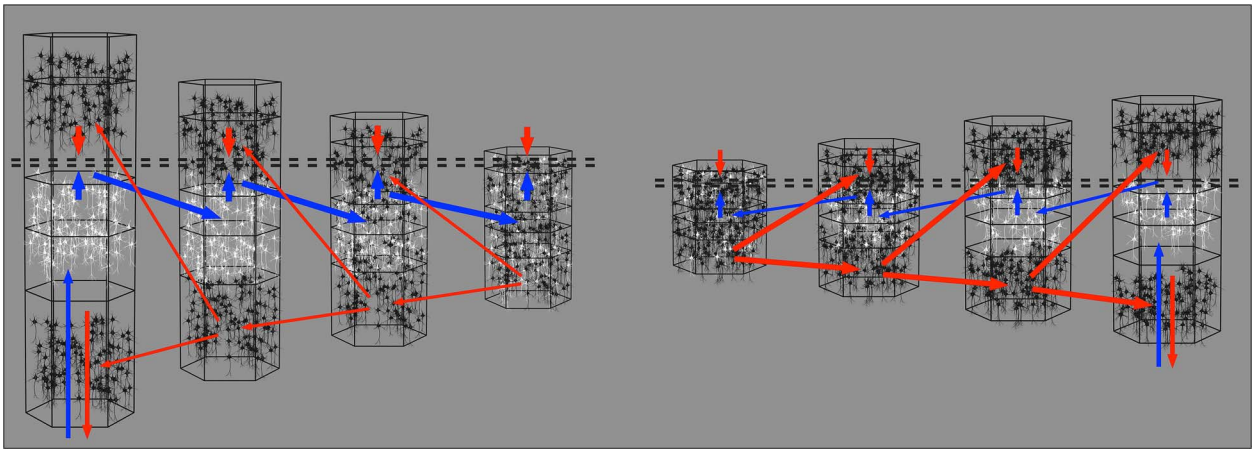

Fig. 3. Signal flows along pathways of radial development in the structural model (after Shipp 2007). Left four columns: ventral cortex. Right four columns: dorsal cortex. At the extremes, left and right, are columns in distal neocortex, associated with a special sensory/motor areas. Columns toward the center are progressively more centrally placed and higher in the hierarchical sensory order. Vertical blue arrows in the extreme special sensory columns indicate the projection of primary sensory afferents to cells in layer 4 and descending small red arrows mark efferent projections from layers 5,6 to subcortical systems. In all columns, small blue vertical arrows mark the onward projections of axons preferentially directed toward the surface from layer 4 to layers 2,3. Small red vertical arrows mark counterflows of traffic from layers 2,3. Laterally projecting red arrows indicate cortico-cortical connections descending from higher in the sensory hierarchy to lower. Diagonal blue arrows mark the counterflow of signals from lower to higher hierarchy. Because of the relative thickness and directed axons of layer 4 in the ventral cortex, interactions in depth between layers 4 and 2,3 are greater in ventral cortex. The double dashed lines shows the zone for development of a Markov blanket.

Further evolutions of connections

Two further trends follow as cell differentiation along the radial lines proceeds.

The emergence of modular columnar structure

As indicated previously, two classes of neuron with differential preferences for space frequency and movement sensitivity develop. To proceed toward maximization of synchrony and minimization of free energy, symmetric bidirectional monosynaptic connections must emerge within and between cells of both classes. This requires emergence of a periodic structure, as will be discussed in detail in a following section.

Circumferential cortico-cortical connections

Mirror assemblies maximizing joint synchrony can arise in another way as cortico-cortical connections develop, superimposing effects of the distance rule upon the structural model, creating inter-area linkage not only along the radial development of the structural model but also circumferential to lines of growth. These cortico-cortical projections form U-shaped loops in cortical white matter, projecting from one cortical area to its neighbors with mirror symmetry, and recurrent reversals of chirality in a series of inter-areal exchanges (Sereno et al. 1995; Konkle 2021). The corpus callosum is the largest such system, creating connections with mirror reversal between hemispheres.

Self-organization at mesoscale: emergence of mirrored synaptic maps in actual anatomy

Our earlier work (Wright and Bourke 2013, 2016, 2022, 2023, 2024; Wright et al. 2014) considered the development of periodic structure at mesoscale. Simulations of cortical growth indicated that dual mirror systems of connections emerge during development, although when compared to actual anatomy, the appearance of the systems is partially obscured as a consequence of the sparsity of synaptic connection of the neurons, as next explained.

Outcome of growth simulations

Our simulations (Wright and Bourke 2016) considered the lateral extension of excitatory intracortical connections at millimetric scale, simplifying axonal lengths of cells to two populations with long versus short axons. The assumption of differing axonal lengths can now be regarded as the outcome of the competitive processes previously described. Mathematical aspects are covered in the Appendix, and qualitative outcomes of the simulations are described here.

Under operation of a force equilibrium algorithm equivalent to maximization of synchrony or minimization of axonal lengths, or both, it was shown that short axon cells formed clusters surrounded by pools of the long-axon cells, the latter in systems with hexagonal, square, or irregular tiling. Variation of the weight placed upon small-world optimization versus synchrony maximization showed that the clustering of the long-axon cells was partly attributable to small world optimization, but that the organization of the cells remained relatively diffuse. With emphasis on synchrony maximization only, the clustering of the cells was complete. With both factors considered, simulation outcomes varied depending on the absolute and relative lengths of the short versus the long axons. Where all axonal lengths were shorter, and when the long-axon lengths were closer to those of the short axons, then a more diffuse small-world order predominated. With increasing difference of the relative axonal lengths, more clearly columnar structure emerged. This can account for the columnar order of the primary visual cortex, as an aspect of strong selection for cells with short axons generated by interactions of layers 2,3 with 4.

Reconstruction of synaptic dispositions

The outcomes of these simulations permitted reconstruction of synaptic positions as they would emerge in a clearly columnar case; in primary visual cortex (V1). Supplementary material accompanying this paper aids in visualization of the synaptic structures in three dimensions. Figure 4 left shows features of reconstruction in a single cluster of short-axon cells and the long-axon cells surrounding the short-axon cluster. In the

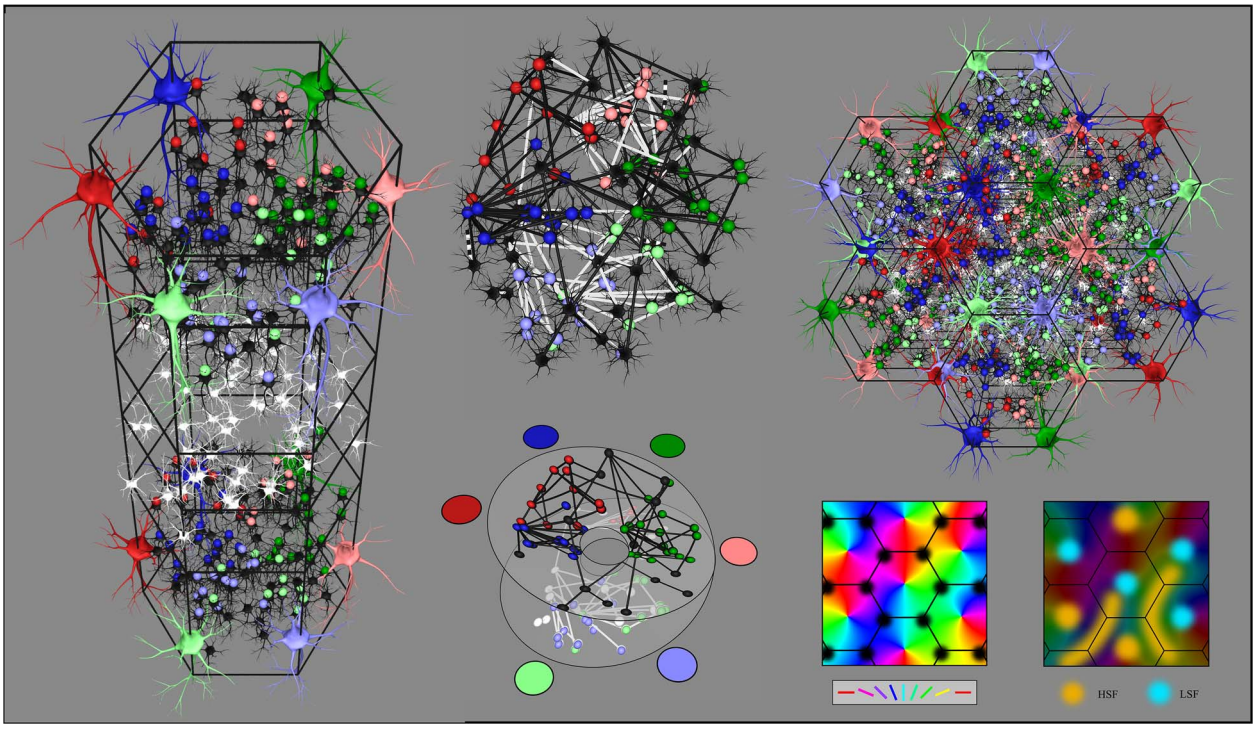

Fig. 4. Organization within cortical columns. Left: reconstruction showing disposition of cells and synapses for maximum synchrony in a surface-oblique view of a column. Large colored neurons represent superficial patch cells. Black smaller cells are local short-axon excitatory cells in layers 2,3 and 5,6. White cells are those of layer 4. Small colored spheres represent synapses efferent from patch cells of the same color (return bidirectional synaptic connections not shown). Middle top: a subset of local cells from the reconstruction are shown in isolation. Black and white connections indicate the way that interpenetration of networks of local cells arises as a consequence of network sparsity. Occasional cross-links are shown as dashed black and white. These bridge the sparse networks and result in amplification of synchrony in closed loops. Middle bottom: an abstract representation of the networks; middle top shows the cells as arrayed in a closed loop configuration analogous to a Mobius strip. Patch cells (shown as colored blobs) deploy synapses so to maximize co-resonance between local and patch cells, thus further maximizing network synchrony. Right top: a view from the cortical surface of adjacent columns, showing how these become arranged in approximate mirror symmetry with their neighbors. Overlap of columns minimizing axonal lengths partially obscures the periodic ordering of patch cells and synapses maximizing synchrony. Right bottom: plots of distribution of orientation preference (left) and high and low spatial and temporal frequency preferences (right) that can be explained by these connection patterns.

reconstruction, the original two-dimensional simulation outcome has been generalized to cortical depth, although this should not be understood as a replication of connections identical to those in the superficial layers.

The reconstructions show the way bidirectionally symmetric connections maximizing synchrony lead to structures consistent with columnar structure in visual cortex (see 4.5) and the superficial patch network. At a distance, *X*, the axonal density of the short- and long-axon populations is equal. At distances less than *X*, the short axons have higher axonal density, and vice versa for long-axon cells, so the short-axon cells generate maximum synchrony by being clustered together, and the long-axon cells must form smaller local clusters, themselves separated by a distance *X* or more—thus able to maximize synchrony over longer ranges by connections skipping over multiples of *X*. Sparsity of connection requires that the short-axon cells form interpenetrating meshes of connection, occasionally cross-connected, thus maximizing their overall synchrony. The short-axon and long-axon populations form connections at cell body separations equal to *X*, creating arcs of connection between the short-axon cells and their surrounding long-axon partners, deployed in a form analogous to projection of the plane onto a Mobius strip. (Again, see Appendix for further details.)

Relations between columns

The process of arrangement for maximum synchrony can be followed into the arrangement of adjacent cortical columns. In Fig. 4 right, reconstructions of seven adjacent columns in hexagonal array are shown. It can be seen that the extension of connections among the long-axon cells have assumed the form of superficial patch cells and maximization of joint synchrony has resulted in approach to mirror reflection between adjacent columns—a mirror symmetry that is broken in a hexagonal array, but is exact if patch cells are in a square array, as in ocular dominance columns.

Figure 4 right also shows the way that approach to ultra-small world connections cells results in a blurring of the columnar pattern that arises as a consequence of synchrony maximization. However, whether clearly columnar or not, the same modular recurrence is present in all cases.

The superficial patch system, global-to-local maps, and spatiotemporal images

The clustering and connections of the long-axon cells as superficial patch cells provide a communication system conveying signals between scales—that is, mapping from the scale of the patch network to the scale of the cortical column, referred to as a global-to-local mapping. So, a bidirectional mapping between scales which is topologically equivalent to mirror reflection occurs. The bidirectional nature of the global-to-local connections permits both read-in and read-out of signals to storage in the local maps.

Information in the global field is stored in the local map, creating a spatiotemporal image. The mapping can be represented

using complex numbers (see Appendix) as

$$O(P,t) \leftrightarrow o\left(\pm p^2, t - \frac{|P-p|}{v}\right) \quad (7)$$

where O is a pattern of activity at the larger (global) mesoscopic scale and o is the projected image to any given column at the local scale. P are cell positions in the global field expressed as a complex number, and p are corresponding positions of neurons in the local maps—the squared value indicating that the local maps are formed by projection to closed loops of connections with a Mobius strip–like conformation. The symbol ± shows that the local map may form with either left- or right-handed mirror chirality. Time is t, and signals pass in either direction with a time lag $|P-p|/v$ where v is again the speed of transmission. Representation of a projection from the global field onto a Mobius strip–like arrangement shortens the distance and therefore the strength of connection between all homologous points in adjacent columns, adding to maximization of synchrony for the entire cell population. Thus, the global field and the local field are mirror reflections in their topological form, while a geometric mirror reflection applies between columns.

Recalling considerations of the emergence of shape versus movement sensitivity, it can be seen that the short-axon local cells are suited to storing information about stimulus shape, while the longer axon superficial patch cells are more suited to conveying information about movement in the global field. The whole is a system for conveying information about interactions between objects—or when operating as outflows from the local maps, to production of structured outputs delivered in a timed sequence.

Match to experimental findings

The mapping (7) explains a wide range of experimental findings (e.g. Bosking et al. 1997; Rockland and Lund 1983; Issa et al. 2000; Girman et al. 1999; Wiesel and Hubel 1974; Blakemore and Van Sluyters 1974; Obermayer and Blasdel 1993; Takahata et al. 2014; Espinosa and Stryker 2012) as reported in Wright and Bourke (2013, 2016, 2022, 2023). The deployment of synapses between patch and local cells underlie the "like to like" rule that connections of the patch cell system project to surrounding local cells of similar orientation preference (OP) in adjacent pinwheels (Bosking et al. 1997)—including recent findings leading to revisions of the rule (Chavane et al. 2022). They account for the organization of OP for slow-moving visual lines oriented from 0 to 180 degrees around the entire 360 degrees of the singularity, and for OP linear zones and saddle points as marginal effects in mirrored systems. Time lags of conduction explain the variation of OP with the speed, length, and angle of attack of the moving line (Basole et al. 2003)—an effect not accounted for in feedforward models of OP, showing that lateral contextual connections exert a major effect, contrasting with the invariant quality of OP in purely feedforward models (Vidyasagar and Eysel 2015).

The deployment of zones of preference for high spatial and temporal frequency (HSF) and low spatial and temporal frequency (LSF) (Issa et al. 2000, 2008; Baker 1990) are also explained. HSF zones form preferentially in circumferential arrangement about singularities because of the concurrent arrival of pulse trains from positions circumferential to the singularity in the global map and vice versa for LSF. Competition for the formation of synaptic connections of either type occurs at the OP singularities, explaining why LSF and HSF appear to be randomly located at the singularities. HSF and LSF zones fit requirement for the occurrence of distinct spatial eigenmodes, tuned to different spatial and temporal frequencies.

Receptive fields of neurons in somatosensory cortex obtained from vertical electrode penetrations show a pattern consistent with the distribution synapses in a Mobius-like configuration (Wright et al. 2014).

The model also accounts for the antenatal development of neuron preferences before exposure to sensory stimulation (Wiesel and Hubel 1974) as well as the postnatal loss of cells in subjects selectively deprived of stimuli with lines of a particular orientation (Blakemore and Van Sluyters 1974). This is because the synaptic ordering shown in Fig. 4 forms without requiring structured inputs, whereas postnatally, ongoing competition results in restriction of responses to stimuli actually present in the environment.

Mirror assemblies of all sorts and their Markov blankets

Figure 5 summarizes the ways in which mirror systems with intervening Markov blankets can arise. As well as mirroring along the radial axes of the structural model, a multitude of mirror systems can tile the cortex, as adjacent columns, as interpenetrating sparse systems equivalent to columns, or as systems separated but interconnected by cortico-cortical connections. They can be mirrored in cortical depth with each layer laterally mirrored. They form mirrors between scales, as the patch system projects to each column or its noncolumnar equivalent, and as mirrors between entire cortical areas. These differing ways in which mirrors can be arranged are a set of topographies corresponding to the topology of the theoretical unit in Fig. 2.

The development of whole brain functionality

The merging of limbic and neocortical function, with capacity for reaction to surprise

By self-evidencing along the Markov blanket running between layers 2, 3 and 4 along the radial lines of development, continuous integration of function can take place. A basis is provided for the fusion of innate behaviors, evolved over millennia, with flexible individual capacities for learning. Subcortical and limbic circuits, sensing viscero-somatic and metabolic needs, and driving elementary approach and avoidance behaviors can be brought into line with the neocortex, with its detailed sensory and perceptual processes, including nociception and two-way interaction with the environment. Blankets forming elsewhere are essentially assisting in the approach to stable exchanges with minimum prediction error along these crucial radial lines.

At all stages, the sudden introduction of unanticipated external stimuli will disrupt these blankets, conveying waves of excitation/inhibition along the radial lines of development, driving return response from the limbic system, and forcing new departures in neocortical self-organization. The merging of innate learning with individual experience and the generation of arousal in response to surprise set the stage for adaptive learning in general. Factors determining the individual's survival and opportunities for alternative plans of action are brought into play together, leading toward outcomes consistent with species survival as well as current and past individual experience.

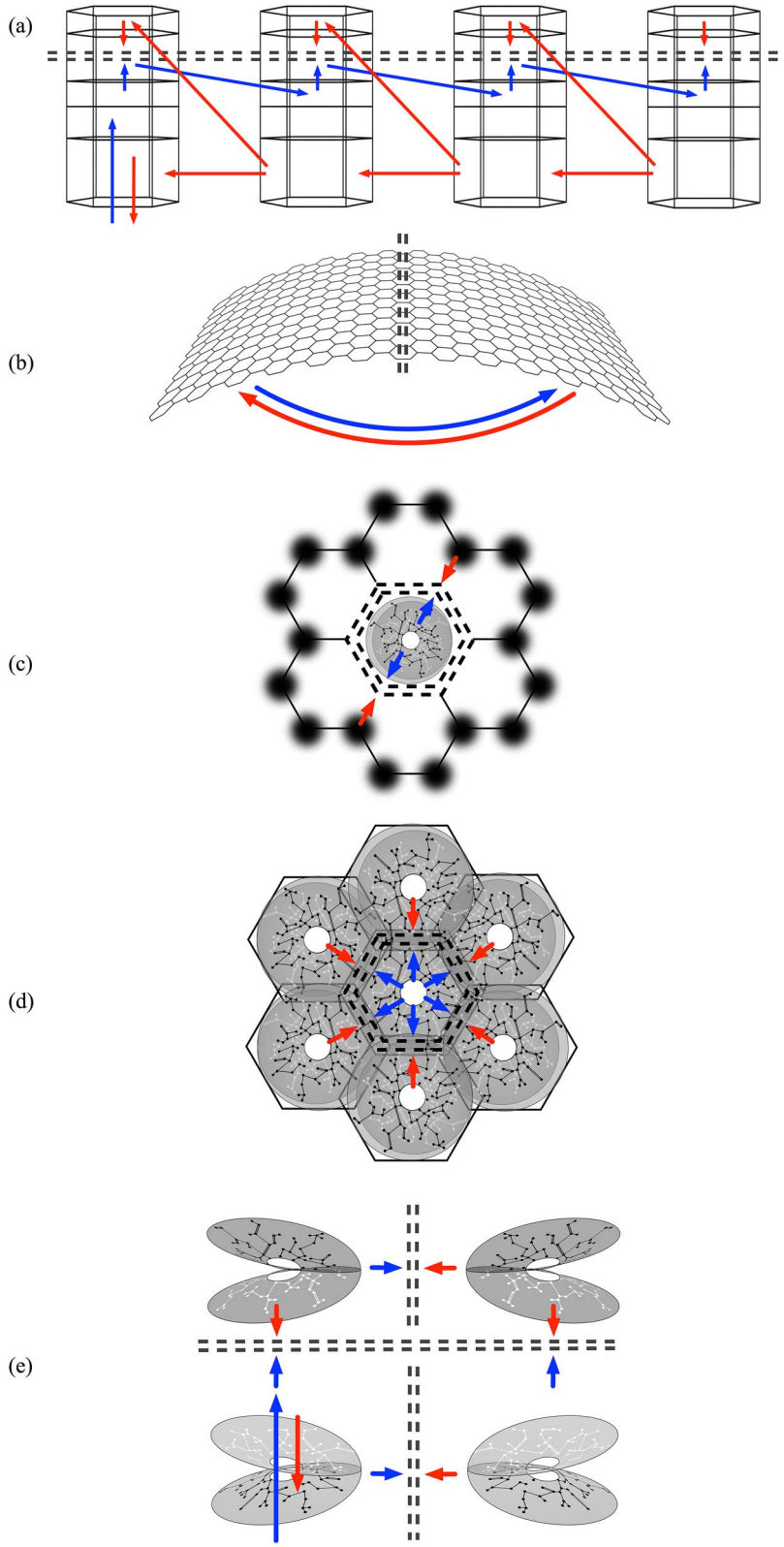

Fig. 5. Mirror representations in approximate developmental sequence. Double black dashed lines indicate lines of mirror symmetry, and associated Markov blankets. Red and blue arrows indicate presynaptic flows toward and along lines of symmetry. (a) Development along the radial lines of the structural model creates a counterflow with an intervening Markov blanket. (b) Additional circumferential development between cortical areas via U-shaped mirror connections projects each cortical area to its neighbors with mirror symmetry. (c) Superficial patch cells shown as dark patches form a communication network generating local maps, producing a mirroring between scales. (d) Adjacent local maps, with variable degrees of overlap, interact between homologous mapping positions across blankets. (e) Along the lines of radial development, mirror pairs form laterally in layers 2,3 and layers 5,6.

Active inference, active affordance, and changes in the level of variational free energy

With surprise and the generation of arousal, a surge in cortical free energy results. As this declines under ongoing free energy minimization, the interaction of all cortical areas must take place. Interactions between dorsal and ventral divisions with minimization of prediction errors mean the creation and fusion of new perceptions, new actions, and plans of action—that is, to active inference and active affordance.

It was earlier described how the greater thickness of layer 4 in the ventral division results in the dorsal division's emphasis on long wavelength movement and timing-sensitive information storage, while in the ventral division the emphasis is on stimulus integrity and the representation of objects. The reversible mapping (7) indicated that these neuron preferences also account for spatially coordinated action schemas, explaining Tucker and Luu's descriptions of the specialized functions of the divisions. The two divisions are specifically suited to cooperation in the merging of active affordance into actions and to active inference.

Conclusion

Limbic and neocortical integration

We have shown how synaptic flow in the developing neocortex, requiring relatively little exact genetic specification, can lead step-by-step to the unfolding of detailed modular structure and function. During this development, self-evidencing keeps the rigid specifications of old brain function in step with flexible neocortical development, leading to a universality at multiple scales of mirrored systems with intervening Markov blankets, mediating active inference and active affordance. This supplements the functional interpretation of the structural model advanced by Luu and Tucker (2023) that utilized the canonical model of prediction error minimization within the cortical column (Bastos et al. 2012, 2020) and now places the interaction of neural systems across internal Markov blankets on a more general and functionally richer basis. Increase of variational free energy in response to surprise aids search, while interactions between mirror connections across Markov blankets of differing geometric form, between and within scales, lead toward maximum mutual information in all areas of the brain.

Simplicity and generality

This theoretic account of neurodevelopment and function is composed of simple elements. Only elementary individual neuron properties needed to be assumed—simple dendritic summation and axonal transmission, Hebbian plasticity on fast and slow timescales, and anti-Hebbian normalization of synaptic gains. The modular organization of the emergent system requires updating at limited numbers of synapses at each time interval—specifically those asymmetrical connections linking the template antenatal systems of closed resonance.

The broad range of application of the free energy principle across disciplinary boundaries is again apparent. Our model reduces to rules for steady-state equilibrium in a nonlinear system subject to modification by memory storage. The emergent patterns of mirror-symmetric flows are reminiscent of patterns of flow in turbulence and other nonlinear systems (Deco and Kringelbach 2020; Tsuda and Fujii 2004) and the maximization of mutual information across brain areas is analogous to the synthesis of material in Large Language models.

Questions arising

The canonical model versus mirrors and Markov blankets

The canonical models for prediction error minimization within the cortical column proposed by Bastos et al. (2012, 2020) offer specific instances of arrangement of neural connections that would achieve generation of a Markov blanket. However, the exact circuits proposed in this class of models do not provide an exhaustive account. They generally suppose the extinction of excitation by an oppositely directed wave of inhibition, whereas our account suggests that interactions between excitatory and inhibitory neurons within each column might at times act to increase bidirectional exchanges of excitation, rather than, and as well as, producing cancelation of excitation by inhibition. This more general explanation of excitatory/inhibitory balance does not preclude a generally greater level of excitatory pulse activity on one side of the blanket or the other since it is synaptic flux that must be symmetrically exchanged, and this can be appropriately adjusted by the fast and slow variation of synaptic gains (equation (2)).

Bastos et al. have also observed that synchronous activity in the gamma band characterizes activity in layers 2,3, whereas activity in layers 4/5 falls in the beta range. They interpret this as a consequence of error correction in the upper layers and smoothing of errors in activity in layers 5,6, enabling an error-corrected and segregated efferent flow to other cortical and subcortical sites. Similar considerations would apply to the present model. Notably, the difference in spectral content between the layers precludes the existence of a Markov blanket between layers 2,3 and 5,6, in contrast to that between layer 2,3 and layer 4.

Growth with apoptotic selection versus detailed genetic controls

As referred to in the Introduction, there are radial gradients for control of genetic expression and molecular factors operating in the structural model. This raises unsolved questions about how these factors might continue to operate in relation to apoptotic selection of neurons on the basis of maximization of synchrony.

Dorsal versus ventral activation systems

Other matters raised in Luu and Tucker (2023) and earlier related papers suggest a further conjecture. These concern the specific actions of the lemnothalamic and collothalamic cortical activation in mediating reaction to surprise, and the associations of these systems with REM sleep and SWS, respectively, including consolidation of memory in sleep. The lemnothalamic activation system's essentially excitatory role, observable as desynchronization of the electrocorticogram, contrasts with the collothalamic system's dopamine mediated role, acting to enhance signal salience (Friston et al. 2012a, 2012b) and thus increasing active affordance. Such bursts of excitation and increase of free energy followed by settling again toward minimum free energy are analogous to the effects of simulated annealing; the procedure used to establish stable states of networks under the Metropolis algorithm (Metropolis et al. 1953). The same roles played by the same systems in REM sleep versus SWS offer opportunity for more sustained surges and following suppression of free energy, and might account for an essential role played by sleep in consolidation of memory.

Testability

The mesoscale model is justified on basis of match to experimental findings largely in V1, but simulation findings indicate general

applicability to all cortical areas, providing an incidental solution of the longstanding mystery of the partially columnar and partially diffuse organization of cortex. Since the model makes specific statements about connectivity at mesoscale, it is subject to ultimate refutation or confirmation by detailed connectome analysis, directed toward detection of recurrent interwoven units with Mobius-like connections, and organization in mirror-dual systems.

Acknowledgments

We thank Professors Karl Friston, Don Tucker, and Miguel Garcia-Cabezas for valued discussion.

Author contributions

James Wright (Conceptualization, Writing—original draft, Writing—review & editing) and Paul Bourke (Software, Visualization).

Supplementary material

Supplementary material is available at *Cerebral Cortex* online.

Funding

This work arose from long-term support including that of the Frank Hixon Fund of the California Institute of Technology, the Mental Health Research Fund (UK) and Wellcome Trust, the United Kingdom, New Zealand, and Australian Medical Research Councils, and the Oakley, and Pratt, Foundations of Australasia.

Conflict of interest statement: None declared.

References

Adams RA, Shipp S, Friston K. Predictions not commands: active inference in the motor system. *Brain Struct Funct*. 2013:218:611–643. https://doi.org/10.1007/s00429-012-0475-5.

Aparicio-Rodriguez G. Garcia-Cabezas MA Comparison of the predictive power of two models of cortico-cortical connections in primates: the distance rule model and the structural model. *Cereb Cortex*. 2023:33:8131–8149. https://doi.org/10.1093/cercor/bhad104.

Baker CL. Spatial- and temporal-frequency selectivity as a basis for velocity preference in cat striate cortex neurons. *Vis Neurosci*. 1990:4:101–113. https://doi.org/10.1017/S0952523800002273.

Barbas H. Pattern in the laminar origin of cortico-cortical connections. *J Comp Neurol*. 1986:252:415–422. https://doi.org/10.1002/cne.902520310.

Barbas H. General cortical and special prefrontal connections: principles from structure to function. *Annu Rev Neurosci*. 2015:38:269–289. https://doi.org/10.1146/annurev-neuro-071714-033936.

Barbas H, García-Cabezas MÁ. How the prefrontal executive got its stripes. *Curr Opin Neurobiol*. 2016:40:125–134. https://doi.org/10.1016/j.conb.2016.07.003.

Barbas H, Garcia-Carbezas MA. Motor cortex layer 4: less is more. *Trends Neurosci*. 2015:38:259–261. https://doi.org/10.1016/j.tins.2015.03.005.

Barbas H, Rempel-Clower N. Cortical structure predicts the pattern of cortico-cortical connections. *Cereb Cortex*. 1997:7:635–646. https://doi.org/10.1093/cercor/7.7.635.

Basole A, White LE, Fitzpatrick D. Mapping of multiple features in the population response of visual cortex. *Nature*. 2003:423:986–990. https://doi.org/10.1038/nature01721.

Bassett DS, Bullmore E. Small-world brain networks. *Neuroscientist*. 2006:12:512–523. https://doi.org/10.1177/1073858406293182.

Bastos AM, Usrey WM, Adams RA, Mangun GR, Fries P, Friston KF. Canonical microcircuits for predictive coding. *Neuron*. 2012:76:695–711. https://doi.org/10.1016/j.neuron.2012.10.038.

Bastos AM, Lundkqvist M, Waite AS, Miller EK. Layer and rhythm specificity for predictive routing. *PNAS*. 2020:117:31459–31469. doi.org/10.1073/pnas.2014868117.

Blakemore C, Van Sluyters RC. Reversal of the physiological effects of monocular deprivation in kittens: further evidence for a sensitive period. *J Physiol*. 1974:237:195–216. https://doi.org/10.1113/jphysiol.1974.sp010478.

Bogacz R. A tutorial on the free-energy framework for modelling perception and learning. *J Math Psychol*. 2017:76:198–211. https://doi.org/10.1016/j.jmp.2015.11.003.

Bosking WH, Zhang Y, Schofield B, Fitzpatrick D. Orientation selectivity and the arrangement of horizontal connections in tree shrew striate cortex. *J Neurosci*. 1997:17:2112–2127. https://doi.org/10.1523/JNEUROSCI.17-06-02112.1997.

Buckley CL, Kim CS, McGregor S, Seth AK. The free energy principle for action and perception: a mathematical review. *J Math Psychol*. 2017:81:55–79. https://doi.org/10.1016/j.jmp.2017.09.004.

Butler AB. Evolution of the thalamus: a morphological and functional review. *Thalamus Relat Syst*. 2008:4:35–58. https://doi.org/10.1017/S1472928808000356.

Chapman CL, Wright JJ, Bourke PD. Spatial eigenmodes and synchronous oscillation: coincidence detection in simulated cerebral cortex. *J Math Biol*. 2002:45:57–78. https://doi.org/10.1007/s002850200141.

Chavane F, Perrinet LU, Rankin J. Revisiting horizontal connectivity rules in V1. *Brain Struct Funct*. 2022:227:1279–1295. https://doi.org/10.1007/s00429-022-02455-4.

Cisek P. Evolution of behavioural control from chordates to primates. *Philos Trans R Soc B*. 2022:377:20200522. https://doi.org/10.1098/rstb.2020.0522.

Conant RC, Ashby WR. Every good regulator of a system must be a model of that system. *Int J Syst Sci*. 1970:1:89–97. https://doi.org/10.1080/00207727008920220.

Constant A. The free energy principle: it's not about what it takes, it's about what took you there. *Biol Philos*. 2021:36:10. https://doi.org/10.1007/s10539-021-09787-1.

Deco G, Kringelbach ML. Turbulent-like dynamics in the human brain. *Cell Rep*. 2020:33:108471. https://doi.org/10.1016/j.celrep.2020.108471.

Downes JH, Hammond MW, Xydas D, Spencer MC, Becerra VM, Warwick K, Whalley BJ, Natsuto SJ. Emergence of a small-world functional network in cultured neurons. *PLoS Comput Biol*. 2012:8:e1002522. https://doi.org/10.1371/journal.pcbi.1002522.

Espinosa JS, Stryker MP. Development and plasticity of the primary visual cortex. *Neuron*. 2012:75:230–249. https://doi.org/10.1016/j.neuron.2012.06.009.

Fields C, Levin M. Somatic multicellularity as a satisficing solution to the prediction-error minimization problem. *Commun Integr Biol*. 2019:12:119–132. https://doi.org/10.1080/19420889.2019.1643666.

Fields C, Glazebrook JF, Levin M. Principled limits of self-representation for generic physical systems. *Entropy*. 2024:26:194. https://doi.org/10.3390/e26030194.

Friston K. Functional integration and inference in the brain. *Prog Neurobiol*. 2002:68:113–143. https://doi.org/10.1016/S0301-0082(02)00076-X.

Friston K. A theory of cortical responses. *Philos Trans R Soc B Biol Sci*. 2005:360:815–836. https://doi.org/10.1098/rstb.2005.1622.

Friston K. Hierarchical models in the brain. *PLoS Comput Biol*. 2008:4:e1000211. https://doi.org/10.1371/journal.pcbi.1000211.

Friston K. The free energy principle: a unified brain theory? *Nat Rev Neurosci*. 2010a:11:127–138. https://doi.org/10.1038/nrn2787.

Friston K. Is the free-energy principle neurocentric? *Nat Rev Neurosci*. 2010b:11:605. https://doi.org/10.1038/nrn2787-c2.

Friston K. A free energy principle for a particular physics. 2019 eprint arXiv:1906.10184. 2019: https://ui.adsabs.harvard.edu/abs/2019arXiv190610184F.

Friston K. Maps and territories, smoke and mirrors. *Behav Brain Sci*. 2022:45:e195. https://doi.org/10.1017/S0140525X22000073.

Friston K, Ao P. Free energy, value, and attractors. *Comput Math Methods Med*. 2012:2012:937860. https://doi.org/10.1155/2012/937860.

Friston K, Buzsaki G. The functional anatomy of time: what and when in the brain. *Trends Cogn Sci*. 2016:20:500–511. https://doi.org/10.1016/j.tics.2016.05.001.

Friston KJ, Shiner T, FitzGerald T, Galea JM, Adams R, Brown H, Dolan RJ, Moran R, Stephan KE, Bestmann S. Dopamine, affordance and active inference. *PLoS Comput Biol*. 2012a:8:e1002327. https://doi.org/10.1371/journal.pcbi.1002327.

Friston K, Thornton C, Clark A. Free energy minimization and the dark room problem. *Front Psychol*. 2012b:3:130. https://doi.org/10.3389/fpsyg.2012.00130.

Friston K, Levin M, Sengupta B, Pezzulo G. Knowing one's place: a free-energy approach to pattern regulation. *J R Soc Interface*. 2015:12:20141383. https://doi.org/10.1098/rsif.2014.1383.

Friston KJ, Parr T, de Vries B. The graphical brain: belief propagation and active inference. *Netw Neurosci*. 2017:1:381–414. https://doi.org/10.1162/NETN_a_00018.

Friston K, Parr T, Yufik Y, Sajid N, Price CJ, Holmes E. Generative models, linguistic communication and active inference. *Neurosci Biobehav Rev*. 2020:118:42–64. https://doi.org/10.1016/j.neubiorev.2020.07.005.

Friston KJ, Fagerholm ED, Zarghami TS, Parr T, Hipolito I, Magrou L, Razo A. Parcels and particles: Markov blankets in the brain. *Netw Neurosci*. 2021:5:211–251. https://doi.org/10.1162/netn_a_00175.

Froudist-Walsh S, Xu T, Niu M, Rapan L, Zhao L, Margulies DS, Zilles K, Wang X-J, Palomero-Gallagher N. Gradients of neurotransmitter receptor expression in the macaque cortex. *Nat Neurosci*. 2023:26:1281–1294. https://doi.org/10.1038/s41593-023-01351-2.

Garcia-Cabezas MA, Joyce MKP, John YJ, Zikopoulos B, Barbas H. Mirror trends of plasticity and stability indicators in primate prefrontal cortex. *Eur J Neurosci*. 2017:46:2392–2405. https://doi.org/10.1111/ejn.13706.

Garcia-Cabezas MA, Barbas H, Zikopoulos B. Parallel development of chromatin patterns, neuron morphology, and connections: potential for disruption in autism. *Front Neuroanat*. 2018:12:70. https://doi.org/10.3389/fnana.2018.00070.

Garcia-Cabezas MA, Zikopoulos B, Barbas H. The structural model: a theory linking connections, plasticity, pathology, development and evolution of the cerebral cortex. *Brain Struct Function*. 2019:224:985–1008. https://doi.org/10.1007/s00429-019-01841-9.

Garcia-Cabezas MÁ, Hacker JL, Zikopoulos B. A protocol for cortical type analysis of the human neocortex applied on histological samples, the atlas of Von Economo and Koskinas, and magnetic resonance imaging. *Front Neuroanat*. 2020:14:576015. https://doi.org/10.3389/fnana.2020.576015.

Garcia-Carbezas MA, Barbas H. Area 4 has layer IV in adult primates. *Eur J Neurosci*. 2014:39:1824–1834. https://doi.org/10.1111/ejn.12585.

Girman SV, Sauve Y, Lund RD. Receptive field properties of single neurons in rat primary visual cortex. *J Neurophysiol*. 1999:82:301–311. https://doi.org/10.1152/jn.1999.82.1.301.

Gollo LL, Mirasso C, Sporns O, Breakspear M. Mechanisms of zero-lag synchronization in cortical motifs. *PLoS Comput Biol*. 2014:10:e1003548. https://doi.org/10.1371/journal.pcbi.1003548.

Goodale MA, Milner AD. Separate visual pathways for perception and action. *Trends Neurosci*. 1992:15:20–25. https://doi.org/10.1016/0166-2236(92)90344-8.

Hansen JY, Shafiei G, Markello RD, Smart K, Cox SML, Norgaard M, Beliveau V, Wu Y, Gallezot J-D, Aumont E, et al. Mapping neurotransmitter systems to the structural and functional organization of the human neocortex. *Nat Neurosci*. 2022:25:1569–1581. https://doi.org/10.1038/s41593-022-01186-3.

Heck N, Golbs A, Riedemann T, Sun J-J, Lessman V, Luhmann HJ. Activity dependent regulation of neuronal apoptosis in neonatal mouse cerebral cortex. *Cereb Cortex*. 2008:18:1335–1349. https://doi.org/10.1093/cercor/bhm165.

Hohwy J. The self-evidencing brain. *Nous*. 2016:50:259–285. https://doi.org/10.1111/nous.12062.

Hollville E, Romero SE, Deshmukh M. Apoptotic cell death regulation in neurons. *FEBS J*. 2019:286:3276–3298. https://doi.org/10.1111/febs.14970.

Horton JC, Adams DL. The cortical column: a structure without a function. *Philos Trans R Soc B*. 2005:360:837–862. https://doi.org/10.1098/rstb.2005.1623.

Issa NP, Trepel C, Stryker MP. Spatial frequency maps in cat visual cortex. *J Neurosci*. 2000:20:8504–8514. https://doi.org/10.1523/JNEUROSCI.20-22-08504.2000.

Issa NP, Rosenberg A, Hussson TR. Models and measurements of functional maps in V1. *J Neurophysiol*. 2008:99:2745–2754, 2754. https://doi.org/10.1152/jn.90211.2008.

Izhikevich EM, Desai NS. Relating STDP to BCM. *Neural Comput*. 2003:15:1511–1523. https://doi.org/10.1162/089976603321891783.

Kaschube M, Schnabel M, Lowel S, Coppola DM, White LE, Wolf F. Universality in the evolution of orientation columns in the visual cortex. *Science*. 2010:330:1113–1116. https://doi.org/10.1126/science.1194869.

Keck T, Toyoizumi T, Chen L, Doiron B, Feldman DE, Fox K, Gerstner W, Haydon PG, Hubener M, Lee H-K, et al. Integrating Hebbian and homeostatic plasticity: the current state of the field and future research directions. *Philos Trans R Soc B*. 2017:372:20160158. https://doi.org/10.1098/rstb.2016.0158.

Kiebel SJ, Friston KJ. Free energy and dendritic self-organization. *Front Syst Neurosci*. 2011:5:80. doi.org/10.3389/fnsys.2011.00080.

Kirchhoff M, Parr T, Palacious E, Friston K, Kiverstein J. The Markov blankets of life: autonomy, active inference and the free energy principle. *J R Soc Interface*. 2018:15:20170792. https://doi.org/10.1098/rsif.2017.0792.

Konkle T. Emergent organization of multiple visuotopic maps without a feature hierarchy. *bioRxiv*. 2021. https://doi.org/10.1101/2021.01.05.425426.

Levin M. The computational boundary of a "self": developmental bioelectricity drives multicellularity and scale-free cognition. *Front Psychol*. 2019:10:2688. https://doi.org/10.3389/fpsyg.2019.02688.

Levitt JB, Lund J, Lund JS. Intrinsic connections in mammalian cerebral cortex. In: *Cortical areas*. CRC Press. eBook ISBN 9780429219108 2002. https://doi.org/10.1201/9780203299296.ch7.

Loonen AJM, Ivanova SA. Circuits regulating pleasure and happiness. The evolution of the amygdala-hippocampal-habenular connectivity in vertebrates. *Front Neurosci*. 2016:10:539. https://doi.org/10.3389/fnins.2016.00539.

Luu P, Tucker DM. Continuity and change in neural plasticity through embryonic morphogenesis, fetal activity-dependent synaptogenesis and infant memory consolidation. *Dev Psychobiol*. 2023:65:e22439. https://doi.org/10.1002/dev.22439.

Luu P, Tucker DM, Friston K. From active affordance to active inference: vertical integration of cognition in the cerebral cortex through dual subcortical control systems. *Cereb Cortex*. 2024:34:bhad458. https://doi.org/10.1093/cercor/bhad458.

Markov NT, Misery P, Falchier A, Lamy C, Vezoli J, Quilodran R, Gariel MA, Giroud P, Ercsey-Ravasz M, Pilaz LJ, et al. Weight consistency specifies regularities of macaque cortical networks. *Cereb Cortex*. 2011:21:1254–1272. https://doi.org/10.1093/cercor/bhq201.

Martin KAC, Roth S. Rusch ES, Superficial layer pyramidal cells communicate heterogeneously between multiple functional domains of cat primary visual cortex. *Nat Commun*. 2024:5:5252. https://doi.org/10.1038/ncomms6252.

Meng Y, Tanaka S, Poon C-S. Comment on universality in the evolution of orientation columns in the visual cortex. *Science*. 2012:336:413. https://doi.org/10.1126/science.1205737.

Metropolis N, Rosenbluth AW, Rosenbluth MN, Teller AH, Teller E. Equation of state calculations by fast computing machines. *J Chem Phys*. 1953:21:1087–1092. https://doi.org/10.1063/1.1699114.

Molnar Z. Cortical columns. In: Rubenstein JLR, Rakic P, editors. *Comprehensive developmental neuroscience: neural circuit development and function in the brain*, vol. 3, pp. 109–129 Amsterdam: Elsevier. 2020. https://doi.org/10.1016/B978-0-12-397267-5.00137-0

Muir DR, Douglas RJ. From neural arbours to daisies. *Cereb Cortex*. 2011:21:1118–1133. https://doi.org/10.1093/cercor/bhq184.

Muir DR, Da Costa NMA, Girardin CC, Naaman S, Omer DB, Ruesch E, Grinvald A, Douglas RJ. Embedding of cortical representations by the superficial patch system. *Cereb Cortex*. 2011:21:2244–2260. https://doi.org/10.1093/cercor/bhq290.

Obermayer K, Blasdel GG. Geometry of orientation and ocular dominance columns in monkey striate cortex. *J Neurosci*. 1993:13:4114–4129. https://doi.org/10.1523/JNEUROSCI.13-10-04114.1993.

Palacios ER, Razi A, Parr T, Kirchoff M, Friston K. On Markov blankets and hierarchical self-organisation. *J Theor Biol*. 2020:486:110089. https://doi.org/10.1016/j.jtbi.2019.110089.

Parr T, Pezzulo G, Friston KJ. *Active inference: the free energy principle in mind brain and behaviour*. Cambridge, Massachusetts: MIT Press; 2022. https://doi.org/10.7551/mitpress/12441.001.0001.

Perin R, Berger TK, Markram H. A synaptic organizing principle for cortical neuronal groups. *Proc Natl Acad Sci USA*. 2011:108:5419–5424. https://doi.org/10.1073/pnas.1016051108.

Puelles L, Alonso A, Garcia-Calero E, Martinez-de-la-Torre M. Concentric ring topology of mammalian cortical sectors and relevance for patterning studies. *J Comp Neurol*. 2019:527:1731–1752. https://doi.org/10.1002/cne.24650.

Puelles L, Alonso A, Garcia-Calero E. Genoarchitectural definition of the adult mouse mesocortical ring: a contribution to cortical ring theory. *J Comp Neurol*. 2024:532:e25647. https://doi.org/10.1002/cne.25647.

Rakic P. Neurogenesis in adult primate neocortex: an evaluation of the evidence. *Nat Rev Neurosci*. 2002:3:65–71. https://doi.org/10.1038/nrn700.

Ramstead MJD, Sakthivadivel DAR, Heins C, Koudahl M, Millidge B, Da Costa L, Klein B, Friston KJ. On Bayesian mechanics: a physics of and by beliefs. *Interf Focus*. 2022:13:20220029. https://doi.org/10.1098/rsfs.2022.0029.

Rockland KS, Lund JS. Intrinsic laminar lattice connections in primate visual cortex. *J Comp Neurol*. 1983:216:303–318. https://doi.org/10.1002/cne.902160307.

Ruiz-Cabrera S, Perez-Santos I, Zaldivar-Diez J, Garcia-Cabezas MA. Expansion modes of primate nervous system structures in the light of the Prosomeric model. *Front. Mammal Sci*. 2023:2. https://doi.org/10.3389/fmamm.2023.1241573.

Sancha-Velasco A, Uceda-Heras A, Garcia-Cabezas MA. Cortical type: a conceptual tool for meaningful biological interpretation of high-throughput gene expression data in the human cerebral cortex. *Front Neuroanat*. 2023:17:1187280. https://doi.org/10.3389/fnana.2023.1187280.

Sang IEWF, Schroer J, Halbhuber L, Warm D, Yang J-W, Luhmann HJ, Kilb W, Sinning A. Optogenetically controlled activity pattern determines survival rate of developing neocortical neurons. *Int J Mol Sci*. 2021:22:6575. https://doi.org/10.3390/ijms22126575.

Sanides F. Architectonics of the human frontal lobe of the brain. With a demonstration of the principles of its formation as a reflection of phylogenetic differentiation of the cerebral cortex. *Monogr Gesamtgeb Neurol Psychiatr*. 1962:98:1–201PMID: 13976313. https://doi.org/10.1007/978-3-642-86210-6_1.

Sanides F. The cyto-myeloarchitecture of the human frontal lobe and its relation to phylogenetic differentiation of the cerebral cortex. *J Hirnforsch*. 1964:47:269–282 PMID 14227452.

Sanides F. Functional architecture of motor and sensory cortices in primates in the light of a new concept of neocortex evolution. In: Noback CR, Montagna W, editors. *The primate brain: advances in primatology*. New York (NY): Appleton-Century-Crofts Educational Division/Meredith Corporation; 1970. pp. 137–208.

Sereno MI, Dale AM, Reppas JB, Kwong KK, Belliveau JW, Brady TJ, Rosen BR, Tootell RB. Borders of multiple visual areas in humans revealed in functional magnetic resonance imaging. *Science*. 1995:268:889–893. https://doi.org/10.1126/science.7754376.

Sheth BR, Young R. Two visual pathways in primates based on sampling of space: exploitation and exploration of visual information. *Front Integr Neurosci*. 2016:10:10. https://doi.org/10.3389/fnint.2016.00037.

Shipp S. Structure and function of the cerebral cortex. *Curr Biol*. 2007:17:R443. doi.org/10.1016/j.cub.2007.03.044.

Shipp S, Friston K. Predictive coding: forward and backward connectivity. In: Martin Usrey W, Murray Sherman S, editors. *The cerebral cortex and the thalamus*. Oxford Academic; 2022. p. 436–445. https://doi.org/10.1093/med/9780197676158.003.0041

Song S, Sjostrom J, Reigl M, Nelson S, Chklovskii DB. Highly non-random features of synaptic connectivity in local cortical circuits. *PLoS Biol*. 2005:3:e350. https://doi.org/10.1371/journal.pbio.0030350.

Stenberg D. Neuroanatomy and neurochemistry of sleep. *Cell Mol Life Sci*. 2007:64:1187–1204. https://doi.org/10.1007/s00018-007-6530-3.

Takahata T, Miyashita M, Tanaka S, Kaas JH. Identification of ocular dominance domains in new world owl monkeys by immediate-early gene expression. *PNAS*. 2014:111:4297–4302. https://doi.org/10.1073/pnas.1401951111.

Trevarthan CB. Two mechanisms of vision in primates. *Psychol Res*. 1968:31:299–337. https://doi.org/10.1007/BF00422717.

Tschacher W, Haken H. Intentionality in non-equilibrium systems? The functional aspects of self-organised pattern formation. *New Ideas Psychol*. 2007:25:1–15. https://doi.org/10.1016/j.newideapsych.2006.09.002.

Tsuda I, Fujii H. A complex systems approach to an interpretation of dynamic brain activity I: chaotic itinerancy can provide a mathematical basis for information processing in cortical transitory and nonstationary dynamics. *Computational Neuroscience: Cortical Dynamics*. 2004:3146:109–128. https://doi.org/10.1007/978-3-540-27862-7_6.

Tucker DM, Luu P. Motive control of unconscious inference: the limbic basis of adaptive Bayes. *Neurosci Biobehav Rev*. 2021:128: 328–345. https://doi.org/10.1016/j.neubiorev.2021.05.029.

Tucker DM, Luu P. Adaptive control of functional connectivity: dorsal and ventral limbic divisions regulate the dorsal and ventral neocortical networks. *Cereb Cortex*. 2023:33:7870–7895. https://doi.org/10.1093/cercor/bhad085.

Tucker DM, Luu P, Johnson M. Neurophysiological mechanisms of implicit and explicit memory in the process of consciousness. *J Neurophysiol*. 2022:128:872–891. https://doi.org/10.1152/jn.00328.2022.

Ungerleider LG, Mishkin M. Two cortical visual streams. In: Ingle DJ, Goodale MA, Mansfield RJW, editors. *Analysis of visual behavior*. Cambridge, MA: MIT Press; 1982. pp. 549–586 Cited at https://irp.nih.gov/accomplishments/anatomy-of-perception-identifying-two-visual-streams-in-the-brain.

Vergara RC, Jaramillo-Riveri S, Luarte A, Moenne-Loccoz C, Fuentes R, Couve A, Maldonado PE. The energy homeostasis principle: neuronal energy regulation drives local network dynamics generating behavior. *Front Comp Neurosci*. 2019:13:49. https://doi.org/10.3389/fncom.2019.00049.

Vezoli J, Magrou L, Goebel R, Wang X-J, Knoblauch K, Vinck M, Kennedy H. Cortical hierarchy, dual counterstream architecture and the importance of top-down generative networks. *NeuroImage*. 2021:225:117479. https://doi.org/10.1016/j.neuroimage.2020.117479.

Vidyasagar TR, Eysel UT. Origins of feature selectivities and maps in the mammalian primary visual cortex. *Trends Neurosci*. 2015:38: 475–485. https://doi.org/10.1016/j.tins.2015.06.003.

Wiesel TN, Hubel DH. Ordered arrangement of orientation columns in monkeys lacking visual experience. *J Comp Neurol*. 1974:158: 307–318. https://doi.org/10.1002/cne.901580306.

Wright JJ, Bourke PD. On the dynamics of cortical development: synchrony and synaptic self-organization. *Front Comp Neurosci*. 2013:7:7. https://doi.org/10.3389/fncom.2013.00004.

Wright JJ, Bourke PD. Further work on the shaping of cortical development and function by synchrony and metabolic competition. *Front Comp Neurosci*. 2016:10:10. https://doi.org/10.3389/fncom.2016.00127.

Wright JJ, Bourke PD. Unification of free energy minimization, spatiotemporal energy, and dimension reduction models of V1 organization: postnatal learning on an antenatal scaffold. *Front Comput Neurosci*. 2022:16:16. https://doi.org/10.3389/fncom.2022.869268.

Wright JJ, Bourke PD. The mesoanatomy of the cortex, minimization of free energy, and generative cognition. *Front Comput Neurosci*. 2023:17:12. https://doi.org/10.3389/fncom.2023.1169772.

Wright JJ, Bourke PD. Markov blankets and mirror symmetries – free energy minimization and mesocortical anatomy. *Entropy*. 2024:26:287. https://doi.org/10.3390/e26040287.

Wright JJ, Liley DTJ. Dynamics of the brain at global and microscopic scales: neural networks and the EEG. *Behav Brain Sci*. 1996:19: 285–295. https://doi.org/10.1017/S0140525X00042679.

Wright JJ, Bourke PD, Chapman CL. Synchronous oscillation in the cerebral cortex and object coherence: simulation of basic electrophysiological findings. *Biol Cybern*. 2000:83:341–353. https://doi.org/10.1007/s004220000155.

Wright JJ, Bourke PD, Favorov OV. Mobius-strip-like columnar functional connections are revealed in somato-sensory receptive field centroids. *Front Neuroanat*. 2014:8:8. https://doi.org/10.3389/fnana.2014.00119.

Yang F-C, Dokovna LB, Burwell RD. Functional differentiation of dorsal and ventral posterior parietal cortex of the rat: implications for controlled and stimulus-driven attention. *Cereb Cortex*. 2022:32:1787–1803. https://doi.org/10.1093/cercor/bhab308.

Appendix

Minimization of free energy, $F \to 0$

At each stage of growth, although there are an increasing number, n, of unidirectional flows of presynaptic flux as synaptic and cell numbers are increasing, the total autocorrelation, A, during a relatively short epoch, T, at all lags, τ is

$$A = \frac{1}{2T}\sum_{ij}^{n}\int_{0}^{T}\int_{-\infty}^{+\infty}\varphi_{ij}(t)\varphi_{ij}\,(t-\tau)\,d\tau dt \tag{A1}$$

and for the $\frac{n}{2}$ pairs of bidirectional flows, total cross-correlation, C, is

$$C = \frac{1}{T}\sum_{ij,ji}^{\frac{n}{2}}\int_{0}^{T}\int_{-\infty}^{+\infty}\varphi_{ij}(t)\varphi_{ji}\,(t-\tau)\,d\tau dt \tag{A2}$$

Therefore, free energy, $A - C$, is zero when for all i, j, t, τ,

$$\varphi_{ij}(t)\varphi_{ij}\,(t-\tau) + \varphi_{ji}(t)\varphi_{ji}\,(t-\tau) = \varphi_{ij}(t)\varphi_{ji}\,(t-\tau) + \varphi_{ji}(t)\varphi_{ij}\,(t-\tau) \tag{A3}$$

Self-evidencing

Writing $\varphi_{ij}(t), \varphi_{ij}\,(t-\tau)\,, \varphi_{ji}(t), \varphi_{ji}\,(t-\tau)$ as a, b, c, d in any order, and $p\,(a, b, c, d)$ as their probabilities in an extended time-series conforming to A3, then

$$p\,(a|b\cup c\cup d)\,p\,(b\cup c\cup d) = p\,(b\cup c\cup d|a)\,p(a) \tag{A4}$$

So, all possible combinations of flux distribution satisfy Bayes theorem.

Redundancy and storage

The ratio of total cross-correlation to total autocorrelation of synaptic flux is a measure of the signal-to-noise ratio for synaptic information storage, i.e.

$$\frac{S}{N} = \frac{C}{A} \le 1 \tag{A5}$$

By Nyquist and Shannon–Hartley theorems

$$D = n\log_2\left(1 + \frac{S}{N}\right) \tag{A6}$$

is the number of bits needed to specify the information stored, where n is the number of bits necessary to specify all synaptic states. A corresponding free energy minimizing formulation can be found in Bogacz (2017) and Friston (2008), where the normalization of excitatory and inhibitory synaptic gains is cast as mirroring or modeling the precision (i.e. signal-to-noise ratio) of prediction errors.

If m is the number of bits required to represent the information input from external sources, then 2^{D-m} distinguishable redundant representations can be stored. $D - m \ge 1$ is the lower limit for the emergence of mirror systems. For $n \gg m$ and $\frac{S}{N} \to 1$, the number of redundant representations and mirror systems can be increasingly large.

Shape and movement sensitivities of neurons

Let r be vector distance from a representative cell. Afferent synaptic flux to the cell from surrounding sources is a function of distance of separation, relative density of connections in a specific direction, and lags of transmission, so the afferent flux received from direction r at time t can be approximated as

$$\varphi_{\text{afferent}}(r,t) = \int_0^\infty f(r)\varphi_{\text{efferent}}\left(r, t - \frac{|r|}{\upsilon}\right) dr \tag{A7}$$

where $\varphi_{\text{afferent}}(r,t)$ is afferent flux, $\varphi_{\text{efferent}}$ are fluxes from distant sources, υ is speed of transmission, and

$$f(r) = D(r)e^{-B|r|} \tag{A8}$$

approximates declining connectivity with distance. B is an inverse length constant and $D(r)$ is a directed amplitude factor weighting for density of average connectivity in direction r.

From the Fourier transform of equation (A8),

$$\mathcal{F}(k) = \frac{DB}{\pi\left(k + B^2\right)} \tag{A9}$$

where k is wavenumber and $\mathcal{F}(k)$describes the spatial components in the field sensed by the afferent cell. Variance of the delays from efferent sources to afferent presynaptic flux is

$$\mathbf{var}\,\varphi_{\text{afferent}} = \left(\frac{D}{B}\right)^2 \tag{A10}$$

This variance determines a bandwidth for sensitivities to time variations in afferent pulses.

Flux exchanges at the boundary of the counterflow Markov blanket occur along the line of interaction of lateral and depth presynaptic flows. These receive lateral cortico-cortical afferents from layers 2,3 and 5,6, and upward flow from layer 4, so their synaptic afference is

$$\begin{aligned}\varphi_{\text{afferent}} = &\int_0^\infty f(r_L)\,\varphi_{\text{efferent}}\left(r_L, t - \frac{|r_L|}{\upsilon}\right) dr_L \\ &+ \int_0^\infty f(r_V)\,\varphi_{\text{efferent}}\left(r_V, t - \frac{|r_V|}{\upsilon}\right) dr_V\end{aligned} \tag{A11}$$

the subscripts L and V indicating parameters of the lateral and depth flows, respectively. In ventral cortex, the parameter $D(r_V)$ is more biased from cortical depth toward the superficial layers by the direction of axons from deep to superficial in layer 4, and parameter B_υ is correspondingly higher since extended lateral flows make relatively little contribution. Since bidirectional connectivity will develop preferentially between cells with a similar predominance of lateral versus deep-to-superficial axonal distribution, then competitive pressure for survival against apoptosis will lead to populations of cells in layers 2,3 with differing lateral axonal range.

As $B \rightarrow$ **large**, information regarding all spatial Fourier components of the input field tend to equality, and afferent presynaptic pulse variance is small. The cell is sensitive to shape in the stimulus field and insensitive to movement. As $B \rightarrow$ **small**, afferent information regarding global field low space-frequencies predominates, and presynaptic pulse variance increases. The afferent cell is insensitive to stimulus shape but sensitive to stimulus movement. Therefore, in ventral cortex cell sensitivity will be toward shape, not movement. For the opposite reasons, sensitivity is biased toward movement, not shape, in the dorsal cortex.

Ongoing formation of columns

The characteristics of the two populations of cells that emerge from the competitive selection can described by

$$\rho_\alpha = N_\alpha\lambda_\alpha \exp\left[-\lambda_\alpha x\right] \tag{A12}$$

$$\rho_\beta = N_\beta\lambda_\beta \exp\left[-\lambda_\beta x\right] \tag{A13}$$

where $\rho_\alpha\ (x), \rho_\beta(x)$ are respective normalized densities of the axonal trees of long-axon, α cells, and short-axon, β cells, as a function of distance, x, from their cell somas. The fraction of presynapses generated by the two cell types are N_α, N_β, and $\lambda_\alpha, \lambda_\beta$ are their axonal inverse length constants.

Bidirectional connection density, $\rho_{\alpha+\beta}$, for all cells would be a maximum if

$$\rho_{\alpha+\beta}(x) = N_\alpha\lambda_\alpha \exp\left[-\lambda_\alpha x\right] + N_\beta\lambda_\beta \exp\left[-\lambda_\beta x\right] \tag{A14}$$

whereas density of connection in an ultra-small world network, where inter-soma distance is surrogate for increasing order of neighbor separation, is given by $\rho_{\alpha+\beta}(x+k)^{-2}$. Thus, disparity of connection density, $\Delta(x)$, of an ultra-small world system and that of the axonal trees of α and β cells is at best

$$\Delta(x) = (x+k)^{-2} - \left(N_\alpha\lambda_\alpha \exp\left[-\lambda_\alpha x\right] + N_\beta\lambda_\beta \exp\left[-\lambda_\beta x\right]\right) \tag{A15}$$

and competitive processes maximizing synchrony (see below) force further departures in separation of cell bodies from the ultra-small optimum.

At a distance, X, from their cell bodies, the population density of the axonal trees of the short-axon and long-axon cell populations are equal.

$$X = \frac{-\ln\left(\frac{N_\alpha\lambda_\alpha}{N_\beta\lambda_\beta}\right)}{\lambda_\beta - \lambda_\alpha} \tag{A16}$$

As bidirectional monosynaptic connections emerge, they result in global-to-local maps in the form of a Reimann projection

$$P \leftrightarrow p \text{ where } p = \pm\sqrt{-1}k\frac{(P-p_0)^n}{|P-p_0|^{n-1}} + p_0 \tag{A17}$$

P are cell positions in the global field expressed as a complex number, and p are corresponding positions of neurons in the local maps. $(P-p_0)^n/|P-p_0|^{n-1}$ describes angular multiplication by n in the projection from P to p. The factor $\sqrt{-1}k$ defines the rotation by 90 degrees and scale of the projection created by the arcs of synapses, chirality is shown + or −, and p_0 is the center of a short-axon cell cluster. The projection of α cells to β cells from diametrically opposite sides of a local map, each at range X, forces their synapses to be deployed in arcs radiating from the local maps center—either deployed on opposite sides of the center—in which case $n=1$—or both radiating from the center on the same side—in which case $n=2$. The $n=1$ case is a simple Euclidean mapping, whereas $n=2$ is a mapping analogous to the mapping of a plane onto a Mobius strip. The latter arrangement permits greater total synchrony by dint of the longer chains of connection among the sparse, but cross-connected, short-axon networks. Angles in the global field from $0-\pi$ are mapped locally from $0-2\pi$ in the plane view of the column, while global angles from $\pi-2\pi$ are also mapped (on a separate mesh of cells) from $0-2\pi$ in the same view, creating the form of an orientation preference singularity.

Homologous positions in the projections from the global map are also brought into highest contiguity—thus enabling them to form connections further maximizing their joint synchrony. That is

$$p_A \leftrightarrow p_B \text{ where } p_A = +\sqrt{-1}k\frac{(P-p_{0A})^2}{|P-p_{0A}|}+p_{0A}$$
$$\text{and } p_B = -\sqrt{-1}k\frac{(P-p_{0B})^2}{|P-p_{0B}|}+p_{0B} \quad \text{(A18)}$$

where A and B indicate adjacent local maps (columns).

Information in the global field is stored in the local map, creating a spatiotemporal image. The mapping can be represented using complex numbers as

$$O(P,t) \leftrightarrow o\left(\pm p^2, t-\frac{|P-p|}{v}\right) \quad \text{(A19)}$$

where O is a pattern of activity at the larger (global) mesoscopic scale and o is the projected image to any given column at the local scale. Signals pass in either direction with a time lag $|P-p|/v$ where v is the speed of transmission.